FULL PAPER

Multiscale Assembly of Superinsulating Silica Aerogels Within Silylated Nanocellulosic Scaffolds: Improved Mechanical Properties Promoted by Nanoscale Chemical Compatibilization

Shanyu Zhao, Zheng Zhang, Gilles Sèbe, Rudder Wu, Raymond V. Rivera Virtudazo, Philippe Tingaut, and Matthias M. Koebel**

Silica aerogels are amongst the lightest mesoporous solids known and well recognized for their superinsulating properties, but the weak mechanical properties of the inorganic network structure has often narrowed their field of application. Here, the inherent brittleness of dried inorganic gels is tackled through the elaboration of a strong mesoporous silica aerogel interpenetrated with a silylated nanocellulosic scaffold. To this avail, a functionalized scaffold is synthesized by freeze-drying an aqueous suspension of nanofibrillated cellulose (NFC)—a bio-based nanomaterial mechanically isolated from renewable resources—in the presence of methyltrimethoxysilane sol. The silylated NFC scaffold displays a high porosity (>98%), high flexibility, and reduced thermal conductivity (λ) compared with classical cellulosic structures. The polysiloxane layer decorating the nanocellulosic scaffold is exploited to promote the attachment of the mesoporous silica matrix onto the nanofibrillated cellulose scaffold (NFCS), leading to a reinforced silica hybrid aerogel with improved thermomechanical properties. The highly porous (>93%) silica-NFC hybrids displays meso- and macroporosity with pore diameters controllable by the NFCS mass fraction, reduced linear shrinkage, improved compressive properties (55% and 126% increase in Young's modulus and tensile strength, respectively), while maintaining superinsulating properties ($\lambda \leq 20$ mW (m K)$^{-1}$). This study details a new direction for the synthesis of multiscale hybrid silica aerogel structures with tailored properties through the use of alkyltrialkoxysilane prefunctionalized nanocellulosic scaffolds.

Dr. S. Zhao, Dr. Z. Zhang, Dr. P. Tingaut, Dr. M. M. Koebel
EMPA, Swiss Federal Laboratories for Materials Science and Technology
CH-8600, Dübendorf, Switzerland
E-mail: philippe.tingaut@empa.ch; matthias.koebel@empa.ch
Dr. G. Sèbe
University of Bordeaux
LCPO, UMR 5629, F-33600, Pessac, France
Dr. G. Sèbe
CNRS, LCPO, UMR 5629, F-33600, Pessac, France
Dr. R. Wu, Dr. R. V. Riviera Virtudazo
Global Research Center for Environment and Energy Based on Nanomaterials Science (GREEN)
National Institute for Materials Science (NIMS)
Japan Namiki, Tsukuba, Ibaraki 305-0044, Japan

DOI: 10.1002/adfm.201404368

1. Introduction

Silica aerogels are extremely low density nanoporous solids, which are most commonly synthesized through a so-called two-step acid–base catalyzed sol–gel route from tetra-alkoxysilane precursors. The dry mesoporous material is obtained after drying the wet gels under either supercritical or ambient pressure conditions, the latter method requiring a hydrophobic gel surface chemistry. Their morphology consists of a "pearl-necklace"-like hierarchical assembly of silica nanoparticles with dimensions from 5 to 10 nm in an open cell 3D structure.[1–3] These inorganic porous materials have been identified as the most promising future insulation materials because of their low thermal conductivity (λ < 12 mW (m K)$^{-1}$ under ambient conditions) and low flammability.[4,5] However, wide-spread applications of silica aerogels have been hindered by their high production cost and brittle/fragile mechanical properties. Three conventional methods have been reported so far for the efficient reinforcement of silica aerogels, namely (i) chemical cross-linking with reactive molecules or polymers, which aims at covalently bridging the silica nanoparticles together and rendering the interparticle necks stronger,[5,6] (ii) incorporating individualized micro- or nanoscopic objects as a secondary phase into the silica matrix, for example polymer nanoparticles, carbon nanotubes or fibers,[7] glass fibers,[8] ceramic fibers[9] or polymeric nanofibers[3] or (iii) interpenetrating a fibrous 3D scaffold within the silica matrix.[10,11] With the latter strategy, the skeleton of the scaffold forms a continuous framework and mechanically supports the fragile mesoporous silica assembly.[3] The methodology is simple, straightforward, and easy adaptable to large-scale production.[12] Significant improvement in the compressive properties of silica aerogels have been reported, with scaffolds based on fiberglass,[13] polyester,[10] nonwoven polyprolylene,[14] polyimide,[15] electrospun polyurethane,[3]

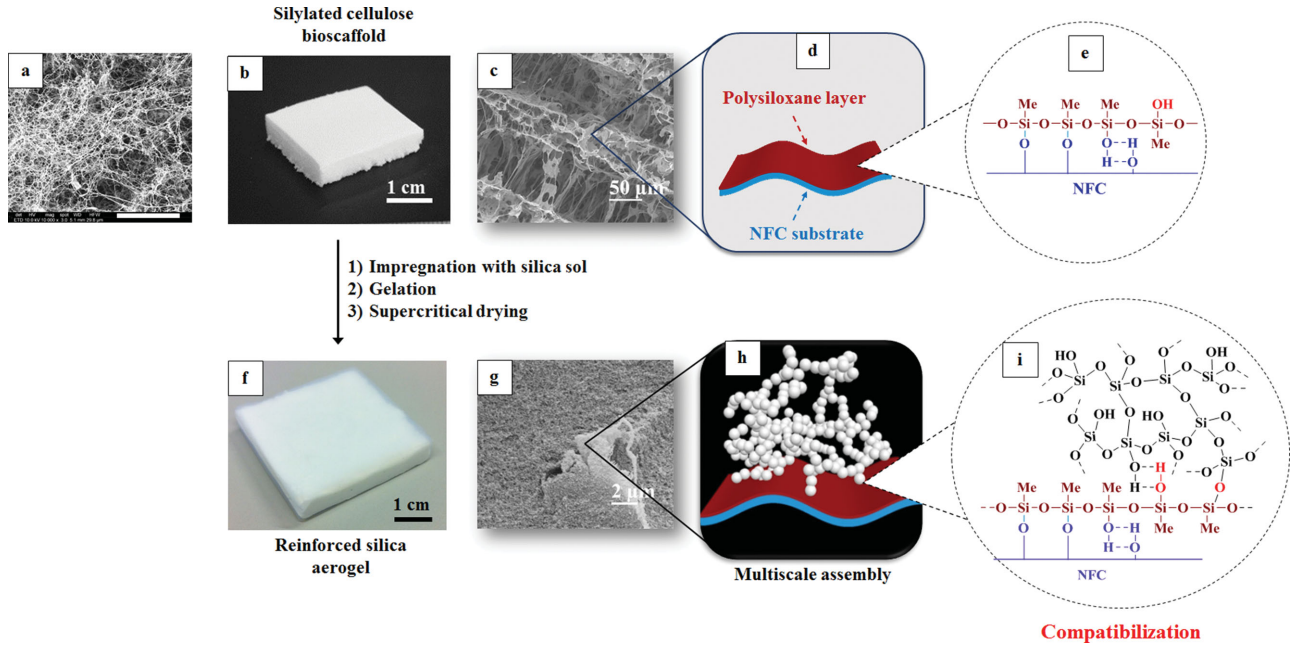

Figure 1. a) SEM image of Nanofibrillated Cellulose (scale bar: 10 µm). b) Photograph of the as-prepared silylated NFCS. c) SEM image of the bioscaffold showing a regular arrangement of NFC sheets into tubular structures. d) Schematic of a NFC sheet structure covered with an MTMS-based polysiloxane layer. e) Proposed chemical structure of silylated NFCS. f) Photograph of a silica aerogel reinforced with silylated NFCS. g) SEM micrograph unveiling the internal hybrid structure of the hybrid aerogel. h) Schematic illustrating the multiscale-assembled mesoporous silica/NFCS interface. i) Schematic illustrating the chemical compatibilization between mesoporous silica network and NFCS surface.

carbon, and ceramic fibers.[16] Among these systems, the ones based on synthetic polyimide (Nylon) or fiberglass (Pyrogel) are commercially available and display superinsulating properties with thermal conductivity as low as 14 mW (m K)$^{-1}$. Very recently, 3D scaffolds based on regenerated cellulose[17–20] or bacterial cellulose[21,22] have been proposed as scaffolds for the reinforcement of silica aerogels. This biocompatible and biodegradable polymer allowed enhancing the mechanical properties of the pristine materials under compressive[17,21] or tensile[20] loading, but thermal conductivity values (λ) above 25 mW (m K)$^{-1}$ were observed as a result of the significantly enhanced skeletal conductivity. [17,19,21,22] To reach simultaneously low thermal conductivities and significantly improved mechanical properties, chemical functionalization strategies can be envisaged to (i) improve the interfacial adhesion between the cellulosic surface and the silica matrix and (ii) reduce the inherent hygroscopicity of the cellulosic scaffold, which generally has a dramatic effect on the thermal conductivity of porous solids.[23]

We have recently reported the facile synthesis of flexible hydrophobic nanocellulosic scaffolds using an efficient procedure based on alkylalkoxysilane chemistry in water.[24] With this method, an aqueous nanofibrillated cellulose (NFC) suspension is freeze-dried in the presence of a methyltrimethoxysilane (MTMS) sol, yielding a highly porous 3D network decorated with a hydrophobic polysiloxane layer at the surface. The starting material used to prepare this silylated scaffold was NFC, which is a renewable biosubstrate isolated from wood or agricultural by-products by mechanical disintegration in water. The process generally involves a high-pressure homogenization step, which promotes the defibrillation of the initial cellulosic substrate (wood or plant pulp, cotton, microcrystalline cellulose) by high mechanical shear.[25] A NFC suspension consists of interconnected cellulose nanofibrils (10–100 nm in diameter with an aspect ratio between 50 and 100) displaying gel-like properties even with solid weight contents of only few percent (**Figure 1**a).[26,27]

In this work, we report the fabrication and characterization of robust mesoporous silica aerogels with superinsulating properties (λ = 13.8–20.9 mW (m K)$^{-1}$) and improved mechanical properties by formation of an interpenetrating network of mesoporous silica within a silylated-nanofibrillated cellulose scaffolds (NFCS) biotemplate. The density and stiffness of the scaffold can be controlled by varying the NFC weight loading in the aqueous suspension before freeze-drying. The NFC surface is compatibilized with the mesoporous inorganic network using a MTMS sol as active silylating agent, while keeping the sol/cellulose ratio constant (Figure 1a–e). An interpenetrating hybrid aerogel structure is obtained by impregnating the silylated NFC scaffold with a tetraethoxysilane (TEOS)-based sol. After gelation, aging and hydrophobization of the silica sol, the resulting gel is dried from supercritical CO_2 (Figure 1f–i). The impact of the NFC scaffold—in both silylated and unmodified variants—on the respective density, linear shrinkage, porosity, Brunauer–Emmett–Teller (BET) surface area, pore volume, average pore diameter, and mechanical properties of the silica aerogel is further described in detail. Finally, the potential of NFCS-silica hybrid aerogel for use in superinsulating materials is discussed in the context of the interplay of the structure and thermomechanical properties.

2. Results and Discussion

NFCS with tailored surface chemistries, reduced hygroscopity, and high flexibility were separately produced in a first step. These scaffolds were later infused with a mesoporous silica gel to produce mechanically robust, superinsulating materials. NFCS were directly prepared by freeze drying of aqueous NFC suspensions in presence of a MTMS sol, resulting in a 3D network of thin cellulose sheets and nanofilaments covered by a polysiloxane layer (Figure 1a–h). Separately, unmodified NFCS were also prepared from NFC suspension in the absence of an MTMS sol to elucidate the effect of the nanoscale chemical compatibilization. The NFC concentration in the initial suspensions was varied from 0.5 to 2.0 wt%, while the MTMS silane percentage within the material (Si wt% as a fraction of the total solid skeletal mass) remained constant, in order to synthesize porous materials with increasing densities but identical molar silane/anhydroglucose ratios of 1.2 (Table S1, Supporting Information). NFCS with three different densities were accordingly produced and labeled according to the NFC concentration in the suspension before freeze-drying. The index "Si" refers to silylated materials (with addition of MTMS sol to the suspension). For instance, unmodified and silylated NFCS prepared with 0.5 wt% NFC are hence labelled NFCS_0.5 and NFCS_0.5_Si, respectively.

The silylation of the NFCS was monitored by FTIR-ATR spectroscopy (**Figures 2**a and S1, Supporting Information). As expected, all modified materials displayed similar spectra, as the silane/cellulose ratio was kept constant in all samples. The characteristic vibrations of the polysiloxane formed after hydrolysis of MTMS appears at 1270 cm^{-1} (δ[C–H]), between 970 and 850 cm^{-1} (ν[Si–OH]), and between 830 and 730 cm^{-1} (ν[Si–C] and/or ν[Si–O]).[24] The core structure of the NFCS's examined by scanning electron microscopy (SEM) reveals a porous macroscopic assembly of thin sheets interconnected by individual nanofilaments, resulting from agglomeration and phase segregation phenomena of nanofibers during the freezing step, when the ice crystals squeezed the cellulosic material. (Figures 2b,c and S2, Supporting Information). The pores size of the NFCS estimated from the micrographs are in the 20–100 µm range. Selected physical properties of the NFCS are summarized in **Table 1**.

The density of the bioscaffold could be controlled by selecting the NFC concentration in the suspension before freeze-drying. For both silylated and nonsilylated NFCS, the apparent density increases with increasing NFC concentration. Addition of the MTMS sol results in a further increase in density and a slight decrease in porosity.[24] The macroporous NFCS exhibit small BET surface areas, low densities and extremely high porosity (≥98%). Due to the presence of large pores in their internal structure (Figure 2b,c), these materials are earmarked by relatively high thermal conductivities in the 30–40 mW $(m\ K)^{-1}$ range. Remarkably, silylated NCFS show slightly lower thermal conductivities than their nonsilylated analogues. We attribute this significant difference to the drastically reduced water uptake of the silylated scaffolds which was quantified by dynamic vapor sorption experiments (Table 1 and Figure S3, Supporting Information). Interestingly, the relative water uptake of the scaffold alone showed to be quite independent of scaffold density but decreased from a maximum value of ≈27% at 95% relative humidity to ≈14.5% upon silylation. Although the impact of moisture on the thermal conductivity was minimized in our study by drying the samples right before the thermal conductivity measurements, the effect of moisture was still quite noticeable.

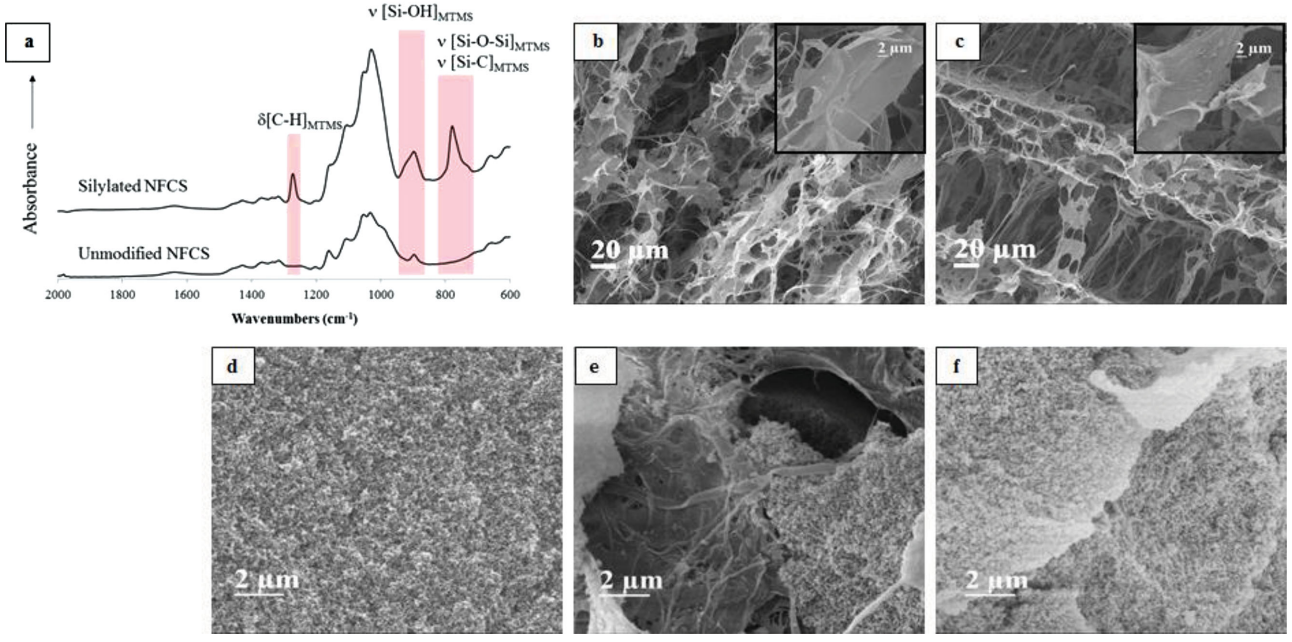

Figure 2. a) FT-IR ATR spectra of unmodified and silylated NFC scaffolds prepared with 2 wt% NFC (NFCS_2.0 and NFCS_2.0_Si, respectively) with ν representing stretching and δ in-plane bending vibrational modes, respectively. b,c) SEM images of NFC_2.0 and NFC_2.0_Si. d–f) SEM images of the fracture surfaces of a reference silica aerogel SA, and the resulting nanocomposites. e) SA_NFC 2.0 and f) SA_NFC_2.0_Si.

Table 1. Volumetric mass density (ρ_{NFCS}), porosity, BET specific surface area, water uptake at 80% relative humidity (RH), and thermal conductivity of the unmodified and silylated NFCS.

NFC scaffolds	Si wt%	ρ_{NFCS} [kg m^{-3}][a)]	Porosity[a)] [%]	BET surface area [m^2 g^{-1}]	Water uptake at 80% RH [g g^{-1}]	Thermal conductivity [mW m K^{-1}]
NFCS_0.5	0	7.4	99.4	24	14.0	33.9
NFCS_1.0	0	10.8	99.3	15	14.5	38.6
NFCS_2.0	0	18.3	98.8	9	14.0	37.2
NFCS_0.5_Si	7.1	9.80	99.4	13	8.0	31.3
NFCS_1.0_Si	7.3	16.4	99.0	7	8.5	34.2
NFCS_2.0_Si	7.9	30.6	98.1	2	8.5	36.3

[a)]See Equations (1)–(4) of the Supporting Information.

The main novelty of this work stems from the casting of a silica sol into a NFC scaffold to produce a robust multiscale aerogel structure with superinsulating properties. We reason that the polysiloxane layer decorating the nanocellulosic scaffold can promote the nanoscale compatibilization of the inorganic silica matrix with the NFCS (Figure 1h), affording a complete overgrowth of the NFC scaffold with a continuous silica phase and resulting in silica aerogels with improved mechanical properties. Accordingly, silica-NFCS hybrid aerogels were produced by impregnation of NFCS samples with a prepolymerized sol derived from TEOS, which had prior been triggered for gelation by addition of catalytic amounts of ammonium hydroxide. The final material was obtained after drying the aged gels from supercritical CO_2. In-line with the nomenclature used for the NFC scaffolds, the resulting silica aerogels are labelled with the prefix "SA" followed by the name of the scaffold they contain. A summary of physical properties of the reference silica aerogel and resulting hybrid materials is given in **Table 2**.

Density, porosity, and linear shrinkage of the silica aerogel reference material (SA_reference) are consistent with data from the literature for silica aerogels prepared under similar conditions.[28] The incorporation of unmodified and silylated NFCS into the silica matrix resulted in hybrid aerogels with densities ranging from 0.122 to 0.146 g cm^{-3}. A progressive decrease in $\Delta L/L$ was noted with increasing W_{NFCS}, i.e., when the density of the NFC scaffold increased (see ρ_{NFCS} in Table 1). This decrease is assigned to the presence of a scaffold of increasing rigidity within the material, which increasingly restrained shrinkage upon drying.

The specific surface area of the aerogels was measured by BET nitrogen sorption (data summary in Table 2 and isotherms in **Figures 3** and S4, Supporting Information). A gradual decrease in the respective surface areas is noted with increasing mass content of the cellulose phase (W_{NFCS}). The specific surface area of the hybrid materials is primarily attributed to the mesoporous silica aerogel. In other words, the addition of the cellulosic fraction with very low surface area (Table 1) to the silica aerogel behaves as a portion of the composite, which does not significantly contribute to the overall surface area. During preparation and processing of NFCS-silica hybrid aerogels, the following effects can influence the specific surface of the final materials (increase ↑ or decrease ↓): (i) the addition of a low surface area biopolymer phase adds "dead mass" and thus lowers the surface area per mass (↓), (ii) the NFC phase stiffens the gel network resulting in reduced shrinkage (see Table 2), thus maintaining a higher mesopore surface area (↑) and (iii) during gelation, a significant part of the colloidal silica in the sol sticks to the NFC phase, forming an overgrowth layer of silica nanoparticles on the scaffold (↓). This fraction of silica is therefore no longer available to build the mesoporous network structure. We believe that at least for the silylated NFCS, mechanisms (i) and (ii) are overcompensated by the densified silica overgrowth layer (iii) as evidenced by electron microscopy

Table 2. Volumetric mass density (ρ_{hybrid}), linear shrinkage ($\Delta L/L$), NFCS mass fraction (W_{NFCS}), SiO_2 mass fraction (W_{SiO2}), porosity, BET specific surface area, pore volume (V_{pore}), and average pore diameter (D_{pore}) of silica aerogels reinforced with unmodified and silylated NFCS (See Equations (5)–(12) of the Supporting Information).

Silica-NFCS hybrids	ρ_{hybrid} [g cm^{-3}]	$\Delta L/L$ [%]	W_{NFCS} [%]	W_{SiO2} [%]	Porosity [%]	BET surface area [m^2 g^{-1}]	V_{pore} [cm^3 g^{-1}]	D_{pore} [nm]
SA_reference	0.133	11.7	0	100	95.0	736	7.1	39
SA_NFCS_0.5	0.122	6.4	5.7	94.3	95.2	726	7.8	43
SA_NFCS_1.0	0.128	6.3	9.0	91.0	94.8	675	7.4	44
SA_NFCS_2.0	0.129	4.7	16.1	83.9	94.5	423	7.3	69
SA_NFCS_0.5_Si	0.130	10.4	6.3	93.7	94.9	631	7.3	46
SA_NFCS_1.0_Si	0.133	9.4	13.3	86.7	94.6	586	7.1	49
SA_NFCS_2.0_Si	0.146	6.9	22.9	77.1	93.7	454	6.42	57

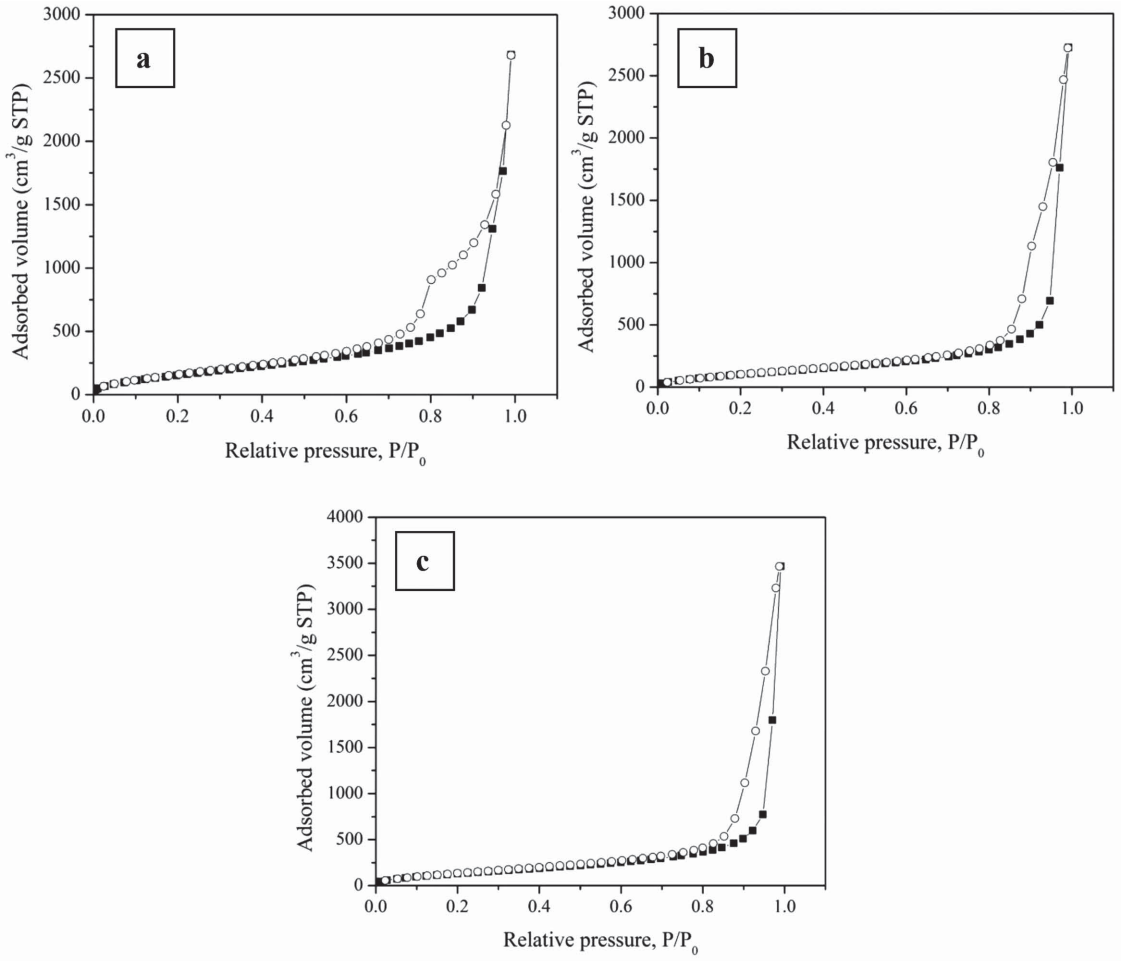

Figure 3. Nitrogen adsorption (black-filled squares) and desorption isotherms (open circles) measured at 77K for a) the reference silica aerogel (SA_reference) and the corresponding multiscale structures b) SA_NFCS_2.0 and c) SA_NFCS_2.0_Si.

images (Figure 2f). Nevertheless, the silica-NFCS hybrids remained highly porous (>93%) and retained their low density. The adsorption/desorption isotherms of all samples display a type IV curve with a hysteresis loop at $P/P_0 > 0.8$, characteristic of mesoporous materials with pores diameter between 2 and 50 nm. No excessive nitrogen uptake is noted when $P/P_0 < 0.05$, suggesting that the materials do not contain micropores (pore diameter below 2 nm). The sharp increase measured in the high relative pressure region of all samples ($P/P_0 = 0.95–1.0$) indicates liquid condensation related to the presence of macropores (pore diameter >50 nm).[29]

The pore volume (V_{pore})—defined as the volume of air per gram of material—and average pore diameter (D_{pore}), were calculated from the volumetric mass densities (ρ_{hybrid}) and BET specific surface areas, respectively (Table 2, see Equations (10) and (11) of the Supporting Information). Barret–Joyner–Halenda and density functional theory methods were avoided in the calculation of pore size and pore size distributions as they are not reliable for the characterization of silica aerogels, due to the mechanical deformation typically observed in silica aerogels in the desorption branch of the capillary condensation range.[28] V_{pore} is not significantly affected by the presence of NFC scaffolds, in agreement with only minor fluctuations in the porosity measured between all samples (between 95% and 93.7%). The respective average pore diameters determined from the pore volumes D_{pore} tend to increase with increasing NFCS mass fraction due to the reinforcing effect of the hybrid structure and reduced shrinkage.[30] All hybrid materials still display mesopore sizes typical for superinsulating silica aerogels (40–70 nm), suggesting that they can retain their low thermal conductivity properties. With regards to the reference aerogel, the assembly of silica particles onto the functionalized scaffolds resulted in multiscale hybrid aerogels displaying meso- and macropores with pore diameters tunable with the NFC scaffold mass fraction.

The presence of NFC scaffolds within the material resulted in a modification of the hysteresis loop, indicative of a change in the extent of the mechanical deformation upon desorption of nitrogen condensed inside the capillaries, thus directly reflecting a difference in the stiffness of the material. The bump in the BET desorption isotherms, which is an indicator for mechanical deformation during desorption and should be thought of an analogous process to ambient pressure drying with an appertaining springback effect—is less pronounced in the hybrid aerogels (Figures 3b,c and S4a–d, Supporting Information) than in the corresponding reference silica aerogel. The

earlier discharge of the liquid sorbent is indicative of both an increase in macropores and network stiffening/strengthening through the scaffold matrix, which is further corroborated by the reduced shrinkage.

Surprisingly, the multiscale aerogel interpenetrated with silylated NFCS displays higher linear shrinkage $\Delta L/L$ values compared with their unmodified counterparts. This phenomenon is attributed to the higher flexibility of the NFCS imparted by the silylation treatment and agrees with the compression tests performed on the native NFCS and silylated scaffolds (Figure S5, Supporting Information).

The effect of the nanoscale compatibilization of the cellulose surfaces is strongly reflected in the mechanical properties of the hybrid aerogels. Cylindrical samples were subjected to uniaxial compression testing. The photographs can be found in Figure S6 (Supporting Information). Representative plots of compressive stress (σ) versus strain (ε), for the SA reference and its hybrids counterparts, are given in **Figure 4**. The deformation of the reference aerogel can be considered elastic below 5% strain and becomes gradually more plastic between 5% and 21.5% strain. Material failure is observed at 23% strain. The compressive modulus (E), maximum compressive strength (σ_{max}) and fracture strain (ε_f) of the sample are in agreement with the values reported in the literature for silica aerogels with similar densities (0.133 g cm^{-3}). [28] The stress–strain curves of the silica hybrids display a similar pattern, but E, σ_{max}, and ε_f values are strongly influenced by the fabrication of the hybrids and even more by the silylation of the NFC surface.

Figure 5 shows a plot of compiled E, σ_{max}, and ε_f data for the SA reference and the NFCS hybrids materials. The presence of unmodified NFC scaffolds within the silica aerogel superstructure causes a deterioration of the mechanical properties, as exemplified by the gradual decrease in E, σ_{max}, and ε_f with increasing NFCS mass fraction (i.e., with increasing density of the cellulosic network). We believe that this behavior is directly related to a poor interfacial adhesion between the cellulosic scaffold and the mesoporous silica. In absence of a nanoscale chemical compatibilization, the NFC-silica interface is highly discontinuous and hence, supports crack propagation and causes a degradation of the mechanical properties instead of the desired reinforcement. Conversely, a significant improvement of mechanical properties is observed when the mesoporous silica is interpenetrated with silylated NFC scaffolds. In that case, nanoscale compatibilization leads to an intimate contact between the silylated template and silica aerogel phases. In comparison with the reference silica aerogel, these hybrids display a maximum increase in E and σ_{max} of 55% and 126%, respectively. Simultaneously, the fracture strain ε_f shows also significant increase at high NFCS mass fraction (30% increase from the SA reference), which indicates a higher internal cohesion within the hybrid structure. The impact of silylation was also noted in the silica aerogels reinforced with NFCS_2.0 and NFCS_2.0_Si, for which buckling was observed. The hybrids containing the unmodified scaffold displayed an early buckling at 5% strain, while silica aerogels reinforced with the silylated structures showed a buckling above 23% strain. The ability of silylated NFC scaffolds to ameliorate both the compressibility and stiffness of silica aerogels is in fact rather unique, since the improvement of an aerogel's compressive properties is normally accompanied with a decrease in densities and E modulus if accomplished by a mere change in the sol concentration.[28] The superior properties displayed by the type of hybrid material studied in this work are attributed to the high interconnectivity of the silylated NFC scaffold embedded inside the aerogel, combined with a nanoscale interface compatibilization effect. Hence, specific interactions between the mesoporous silica and the polysiloxane, which decorates the NFC surface may have occurred upon drying of the hybrid structure, through the eventual formation of siloxane linkages or hydrogen bonds (Figure 1i). Because the density of the NFC scaffold is low in comparison with the aerogel phase and the resulting interpenetrated structures show reduced shrinkage, no clear correlation can be established between their mechanical properties and densities (Figure S7, Supporting Information). It is apparent, however, that the nanoscale compatibilization effect is much more noticeable than the density dependence of the hybrids.

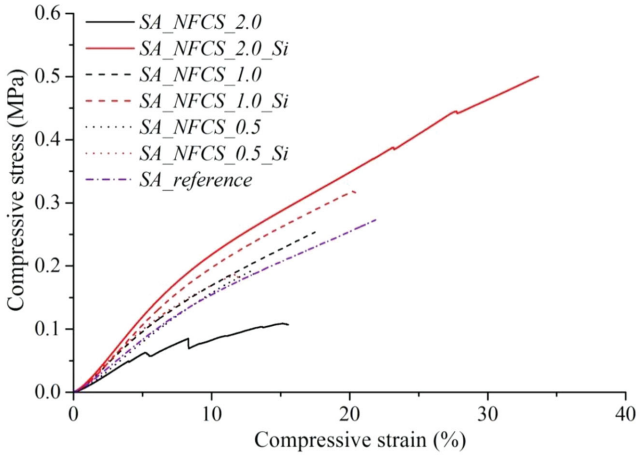

Figure 4. Compressive stress versus strain curves of the reference silica aerogel and the resulting multiscale structures reinforced with unmodified and silylated NFCS.

To further corroborate the impact of the nanoscale compatibilization by the chemical silylation treatment, fracture surfaces of compression tested specimens were analyzed by SEM (Figures 2d–f and S8, Supporting Information). As expected, the fracture surface of the reference material displays typical mesoporous silica aerogel 3D network structure. The SEM pictures of the unmodified SA_NFCS hybrids reveals the presence of fractured silica aerogel clusters linked together by cellulosic sheets and nanofilaments (Figures 2e and S8a,S8c, Supporting Information). There is no indication of an adhering silica layer on the cellulosic substrate, suggesting that the cellulose–silica interface is the weakest link in the structure, thus further supporting the results of the mechanical tests. The fracture surfaces of the silylated SA_NFCS_Si hybrids, on the contrary, strongly resemble that of the reference sample, with its mesoporous silica structure (Figures 2f and S8b,S8d, Supporting Information). The cellulosic scaffold is completely overgrown with the aerogel phase and no cracks are visible along the interface. In conclusion, the introduction of a polysiloxane layer on the NFC surface leads to a nanoscale compatibilization effect, which is essential for the preparation of

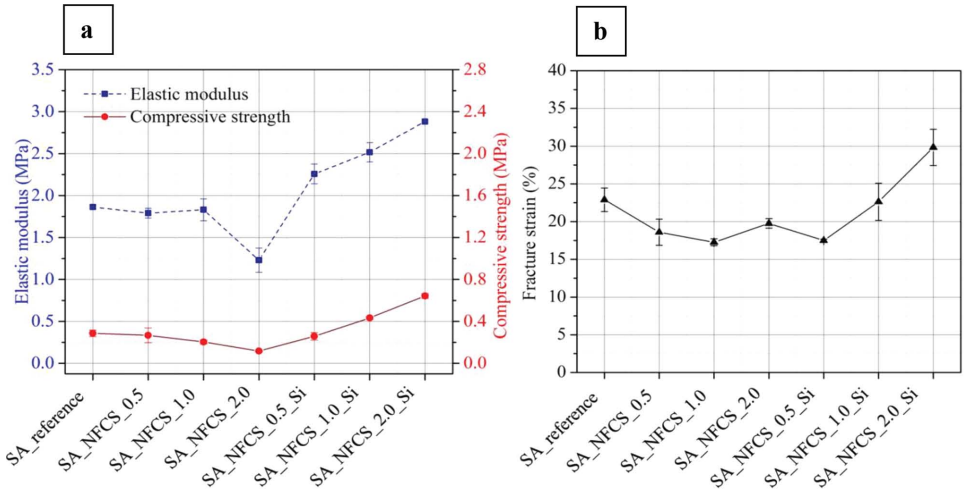

Figure 5. a) Compressive modulus E and maximum compressive strength (σ_{max}) and b) fracture strain (ε_f) of the reference silica aerogel and of the resulting multiscale aerogel structures reinforced with unmodified and silylated NFCS.

aerogel hybrid materials with improved E-modulus, compressive strength and fracture strain.

Aside from mechanical properties, thermal properties of silica aerogels and their hybrids are of great importance for practical applications. Thermal conductivity measurements of monolithic square-shaped tiles were conducted on a home-built guarded hot plate device, especially designed for the analysis of small samples (**Figure 6**). The silica aerogel reference tile exhibits super-insulating properties with a thermal conductivity (λ) of 12.5 mW (m K)$^{-1}$, as expected for a silica aerogel with such density, owing to the reduced gas transport of the pore fluid air, which is trapped inside mesopores smaller than the free mean path of air (70 nm under ambient conditions).[31,32] The incorporation of unmodified NFC scaffolds leads to an increase in thermal conductivity of the material with increasing NFCS mass fraction (scaffold density), which is attributed to the higher solid conduction of the NFCS. A similar trend is observed for the aerogels containing silylated NFCS but lower thermal conductivities were systematically measured despite the higher scaffold density (comparison of samples with similar cellulose/silica ratio in Table 2 and Figure S9, Supporting Information). In comparison, the respective thermal conductivity values of unmodified scaffolds and resulting aerogel hybrids are systematically 2–3 mW (m K)$^{-1}$ higher than those of the corresponding silylated materials of comparable scaffold composition (compare results from Table 1 and Figure 6). We attribute this difference to the drastically reduced hygroscopicity of the silylated scaffolds, as previously discussed (Table 1 and Figure S3, Supporting Information).

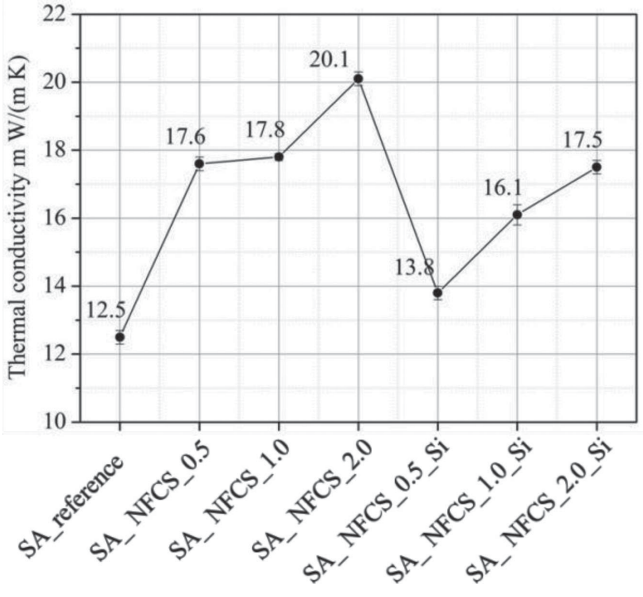

Figure 6. Thermal conductivity values of the reference silica aerogel and resulting multiscale hybrid aerogels containing unmodified and silylated NFCS.

Despite the large scaffold densities and moisture-related differences, all hybrids displayed λ values of 20 mW m K^{-1} or less, which makes them superinsulating materials. Such a performance is remarkable and places these multiscale structures amongst the best ambient condition thermal insulators. In comparison, silica aerogel composites containing regenerated and bacterial cellulose nanofibers at equivalent filler content and density offer far inferior insulation performance.[17,19,21,22] The thermal conductivity values are comparable with cellulose-based aerogels elaborated from surface carboxylated cellulose nanofibers[33] or polymethylsilsesquioxane-urea composites reinforced with cellulose nanofibers,[34] and superior to silica aerogel composites with inorganic or synthetic polymer scaffolds, which generally show lower water uptake than polysaccharides. Together with recently reported superinsulating bio-based aerogels,[33,35] the materials presented here constitutes one of the most advanced biopolymer silica hybrid nanoengineered materials in heat insulation performance.

3. Conclusion

We have presented a novel route to robust mesoporous, nanoengineered biopolymer-silica aerogel hybrids with

superinsulating properties (λ = 13.8–20.1 mW (m K)$^{-1}$) and improved mechanical properties, by forming an interpenetrating silica network inside a silylated nanofibrillated cellulose scaffold (NFCS_Si). The incorporation of unmodified and silylated NFCS into the silica matrix resulted in interpenetrated structures with low density (0.122–0.146 g cm^{-3}), reduced linear shrinkage, high specific surface area (above 450 m^2 g^{-1}) and high porosity (>93%). The resulting multiscale hybrids retained the high mesoporosity, which is characteristic for the silica aerogel phase. When compared with the reference silica aerogel, the best hybrids displayed an increase in compressive modulus (E) and maximum strength (σ_{max}) of 55% and 126%, respectively while maintaining a low thermal conductivity of 17.5 mW m K^{-1}. The ability of silylated NFC scaffolds to concomitantly ameliorate the compressibility and stiffness of silica aerogels is unique and was described for the first time to a nanoscale chemical compatibilization through polysiloxane layer grafted onto the NFC surface. Future characterization of this new type of hierarchical multiscale structures with x-ray tomography will allow us to further elucidate the 3D arrangement of the cellulosic skeleton inside the silica network, and to further corroborate the nanoscale compatibilization effect through in situ mechanical compression testing.

This work demonstrates the importance of modifying the NFC surface when designing mesoporous silica aerogels interpenetrated with nanocellulosic scaffolds. Since a broad library of alkoxysilanes is commercially available, we foresee that silylated NFC could open new opportunities for the design of novel functional aerogels.

4. Experimental Section

Materials and Chemicals: A NFC suspension with a solid content of 7.8 wt% was prepared from oat straw cellulose powder (Jelucel OF300) according to a procedure previously published.[24,27] Research grade PEDS, a prepolymerized form of tetraethoxysilane (TEOS) containing a water-to-TEOS molar ratio of 1.5 and a SiO_2 content of 20% w/w in ethanol (PEDS-P75E20, PCAS, France), was used as the silica gel precursor (See Figure S10, Supporting Information). Hexamethyldisilazane (HMDZ, 98.5%, ABCR, Germany) and methyltrimethoxysilane (MTMS, 98%, Alfa Aesar GmbH & Co KG, Germany) were used as hydrophobizing agents. Ethanol (F25-AF-MEK ethanol denatured with 2% methyl ethyl ketone, Alcosuisse, Switzerland) and heptane (UN 1206, Brenntag, Switzerland) were used as solvents. Hydrochloric acid (HCl, 37%) and ammonium hydroxide solution (NH_3·H2O, 28%–30%) were purchased from Sigma-Aldrich (Switzerland). Deionized water was used in all experiments. All chemicals were used as received without any further purification.

Synthesis of Unmodified and Silylated Bioscaffolds: The NFC suspension with a solid content of 7.8 wt% was diluted to reach concentrations of 0.5, 1.0, and 2 wt% with deionized water, and homogenized with an Ultra-Turrax system set to 11000 rpm for 30 s. The NFC suspensions were subsequently adjusted to a pH of 4 with HCl. The MTMS-based polysiloxane sol was prepared separately. A defined mass of deionized water was first introduced in a beaker and the solution was adjusted to a pH of 4 with HCl. Different amounts of MTMS were added dropwise to the solution and the mixture stirred for 5 min at 500 rpm with a magnetic stirrer. This solution was then added dropwise to the NFC suspension and stirred at room temperature for 2 h. 225 cm^3 of the suspension was poured into a copper box mould (15 × 15 cm) and the rest of the suspension was equally distributed into 7 cylindrical copper tubes (inner diameter: 16 mm) in order to prepare samples with square or cylindrical shapes, respectively. All samples were then frozen with liquid nitrogen and freeze-dried. The MTMS concentration was adjusted to 7.4 mmol $(g_{NFC})^{-1}$ in order to obtain NFC scaffolds with the same silylation level (Table S1, Supporting Information). The resulting unmodified and silylated NFCS were then stored in a desiccator before any utilization.

Synthesis of Silica Hybrids Aerogels: PEDS stock solutions were diluted with ethanol to reach a final silica concentration of 6%. The gelation was triggered by adding 2% by volume of a 5.5 M solution of ammonium hydroxide to the sol, which was then cast into an as-prepared cellulose scaffold specimen, which had previously been placed inside a matching mould. Gelation occurred in approximately 8–10 min after which the alcogels were covered with ethanol and aged overnight. Aging the gels resulted in isotropic shrinkage, which allowed the gels to be removed from the moulds and placed in glass beakers filled with ethanol and covered with aluminum foil. The gels were washed twice with ethanol at 55 °C, followed by exchanging them into heptane twice at 55 °C for 24 h each. Hydrophobic treatment of the silica gel surfaces was carried out by soaking the gels in a heptane solution with HMDZ at 65 °C for 24 h. The imbibed liquid of the gel was exchanged to liquid carbon dioxide and then dried supercritically in a SCF extractor (Autoclave 4334/A21–1, Separex, France). Further, processing consisted of manual grinding of the dried aerogel and hybrids samples to even out the uneven surface left by the minisci caused by the surface tension of the liquid sol liquid state with sandpaper.

SEM Characterization: The NFC bioscaffolds and hybrid aerogels were analyzed by affixing the samples on the sample holder using a carbon pad, followed by coating them with a 7.5 nm-thick platinum layer. SEM analysis of all materials was performed on a FEI Nova NanoSEM 230 instrument (FEI, Hillsboro, Oregon, USA) at an accelerating voltage of 10 kV and a working distance of 5 mm.

Evaluation of Bioscaffolds Density and Porosity: The apparent volumetric mass density of the bioscaffold ($\rho_{Bioscaffold}$) and its porosity was calculated according to Equations (1)–(4) of the Supporting Information.

Water Sorption Experiments: The water sorption isotherms of unmodified and silylated NFC scaffolds were evaluated using a vapor sorption analyzer (VTI-SA+, TA Instruments, New Castle, United States). Prior to measurement, the cellulosic scaffold (≈15 mg) was first dried at 60 °C and 0% RH for 1 h followed by equilibration at 25 °C. The weight of the sample was then recorded at 25 °C as a function of relative humidity, which was increased from 0% to 95%, with increments of 5% (Note that the sample's weight was recorded at equilibrium, i.e., when no weight change lower than 0.01% was noted within 5 min).

Evaluation of the Brunauer–Emmett–Teller (BET) Specific Surface Area of the Bioscaffolds and the Silica Aerogels Hybrids: The BET-specific surface of the cellulosic scaffolds was determined by nitrogen sorption, using a surface area and pore size analyzer, SA 3100 (Beckmann Coulter, USA). About 30 mg of material was dried at 105 °C for 18 h. The nitrogen adsorption was measured at –196 °C, under a range of relative vapor pressures between 0.05 and 0.2. BET-specific surface area was evaluated from the obtained adsorption isotherm. The BET-specific surface area of multiscale aerogels was analyzed via nitrogen gas adsorption/desorption isotherm recorded at 77K by an automatic surface area analyzer (AUTOSORB-iQ, Quantachrome, USA) using a procedure which was optimized for silica aerogel materials.

Evaluation of the Pore Volume, Pore Diameter, and Porosity of Silica Aerogels Hybrids: The pore volume (V_{pore}), average pore diameter (D_{pore}), and porosity of the aerogels were calculated from the density of the aerogel and their specific surface area using Equations (5)–(8) of the Supporting Information.

Evaluation of the Compressive Properties of the NFCS and Silica Aerogel Hybrids: The NFC scaffolds were cut into rectangular specimens of 30 × 30 × 10 mm^3. Prior to measurement, all samples were conditioned at 50% relative humidity and 23 °C for at least 24 h. Compression tests were performed with a Universal Testing System Z010 (Zwick, Germany) equipped with a 200N load cell. The sample was placed between the testing plates and was compressed at a speed of 1 mm min^{-1} to 50% strain and this position held for 10 s before the piston was retracted. Three replicates were measured for each sample. Mechanical characterization of the hybrids were performed on a monolithic

cylindrical sample using a universal materials testing machine (Zwick/Z010, Zwick/Roell, Germany), equipped with a 2kN force transducer (KAP-S, AST Gruppe GmbH, Germany) in a controlled environment (23 °C, 50% relative humidity). Elastic moduli were measured in compression mode and were calculated from the linear region of the stress–strain curves, which typically occurred at 3% ± 2% strain. A constant deformation rate of 1 mm min^{-1} was used and compressive strength values were taken at the first noticeable sign of cracking.

Evaluation of the Thermal Conductivity: Thermal conductivity measurements of square-shaped monolithic tiles of approximately 45 × 45 × 7 mm were carried out on a custom-built guarded hot plate device designed for small samples/low thermal conductivity materials (measuring zone of 25 × 25 mm) with a 15 °C temperature difference. In order to be consistent with measurements according to the European Standards,[36] calibration measurements were carried out using conventional expanded polystyrene samples measured once in a 50 cm × 50 cm calibrated and validated testing equipment. The small guarded hot plate measurement data was then calibrated using these known standards.

Supporting Information

Supporting Information is available from the Wiley Online Library or from the author.

Acknowledgements

This work was financially supported by the European Commission under the Seventh Framework Programme (Call identifier: EeB.NMP.2010–1, Contract No. 260141, Aerocoins project: www.aerocoins.eu).

Received: December 10, 2014
Revised: February 12, 2015
Published online: March 16, 2015

[1] a) S. S. Kistler, *Nature* **1931**, *227*, 741; b) S. S. Prakash, J. C. Brinker, A. J. Hurd, S. M. Rao, *Nature* **1995**, *375*, 431.
[2] A. C. Pierre, G. M. Pajonk, *Chem. Rev.* **2002**, *102*, 4243.
[3] L. Li, B. Yalcin, B. N. Nguyen, M. A. B. Meador, M. Cakmak, *ACS Appl. Mater. Interfaces* **2009**, *1*, 2491.
[4] a) R. Baetens, B. P. Jelle, A. Gustavsen, *Energy Buildings* **2011**, *43*, 761; b) L. W. Hrubesh, *J. Non-Cryst. Solids* **1998**, *225*, 335; c) N. Hüsing, U. Schubert, *Angew. Chem. Int. Ed.* **1998**, *37*, 22; d) D. M. Smith, A. Maskara, U. Boes, *J. Non-Cryst. Solids* **1998**, *225*, 254.
[5] M. A. Aegerter, N. Leventis, M. M. Koebel, *Aerogels Handbook*, Springer, New York, USA **2011**.
[6] a) A. Katti, N. Shimpi, S. Roy, H. Lu, E. F. Fabrizio, A. Dass, L. A. Capadona, N. Leventis, *Chem. Mater.* **2006**, *18*, 285; b) N. Leventis, *Acc. Chem. Res.* **2007**, *40*, 874; c) M. A. B. Meador, L. A. Capadona, L. McCorkle, D. S. Papadopoulos, N. Leventis, *Chem. Mater.* **2007**, *19*, 2247; d) M. A. B. Meador, E. F. Fabrizio, F. Ilhan, A. Dass, G. Zhang, P. Vassilaras, J. C. Johnston, N. Leventis, *Chem. Mater.* **2005**, *17*, 1085; e) G. Zhang, A. Dass, A. M. M. Rawashdeh, J. Thomas, J. A. Counsil, C. Sotiriou-Leventis, E. F. Fabrizio, F. Ilhan, P. Vassilaras, D. A. Scheiman, L. McCorkle, A. Palczer, J. C. Johnston, M. A. B. Meador, N. Leventis, *J. Non-Cryst. Solids* **2004**, *350*, 152.
[7] M. A. B. Meador, S. L. Vivod, L. McCorkle, D. Quade, R. M. Sullivan, L. J. Ghosn, N. Clark, L. A. Capadona, *J. Mater. Chem.* **2008**, *18*, 1843.
[8] C. Y. Kim, J.-K. Lee, B. I. Kim, *Colloid. Surf. A: Physicochem. Eng. Aspects* **2008**, *313–314*, 179.
[9] J. Wang, J. Kuhn, X. Lu, *J. Non-Cryst. Solids* **1995**, *186*, 296.
[10] J. K. Lee, *US20070259979 A1* **2007**.
[11] C. J. Stepanian, G. L. Gould, R. Begag, *US7504346 B2* **2009**.
[12] H. Maleki, L. Duraes, A. Portugal, *J. Non-Cryst. Solids* **2014**, *385*, 55.
[13] B. Yuan, S. Ding, D. Wang, G. Wang, H. Li, *Mater. Lett.* **2012**, *75*, 204.
[14] Z. Zhang, J. Shen, X. Ni, G. Wu, B. Zhou, M. Yang, X. Gu, M. Qian, Y. Wu, *J. Macromol. Sci. Part A* **2006**, *43*, 1663.
[15] D. H. Blount, *US4954327 A* **1990**.
[16] a) A. Karout, P. Buisson, A. Perrard, A. C. Pierre, *J. Sol-Gel Sci. Technol.* **2005**, *36*, 163; b) K. E. Parmenter, F. Milstein, *J. Non-Cryst. Solids* **1998**, *223*, 179.
[17] J. Cai, S. Liu, J. Feng, S. Kimura, M. Wada, S. Kuga, L. Zhang, *Angew. Chem. Int. Ed.* **2012**, *51*, 2076.
[18] M. Litschauer, M.-A. Neouze, E. Haimer, U. Henniges, A. Potthast, T. Rosenau, F. Liebner, *Cellulose* **2011**, *18*, 143.
[19] J. Shi, L. Lu, W. Guo, J. Zhang, Y. Cao, *Carbohydr. Polym.* **2013**, *98*, 282.
[20] S. Liu, T. Yu, N. Hu, R. Liu, X. Liu, *Colloid. Surf. A: Physicochem. Eng. Aspects* **2013**, *439*, 159.
[21] H. Sai, L. Xing, J. Xiang, L. Cui, J. Jiao, C. Zhao, Z. Li, F. Li, *J. Mater. Chem. A* **2013**, *1*, 7963.
[22] H. Sai, L. Xing, J. Xiang, L. Cui, J. Jiao, C. Zhao, Z. Li, F. Li, T. Zhang, *RSC Adv.* **2014**, *4*, 30453.
[23] a) F. Ochs, H. Müller-Steinhagen, presented at *NATO Adv. Study Inst. TESSEC*, Izmir, Cesme **2005**; b) B. Nait-Ali, C. Danglade, D. S. Smith, K. Haberko, *J. Eur. Ceram. Soc.* **2013**, *33*, 2565; c) P. T. Tsilingiris, *Energy Convers. Manage.* **2008**, *49*, 1098.
[24] Z. Zhang, G. Sèbe, D. Rentsch, T. Zimmermann, P. Tingaut, *Chem. Mater.* **2014**, *26*, 2659.
[25] a) P. Tingaut, T. Zimmermann, G. Sebe, *J. Mater. Chem.* **2012**, *22*, 20105; b) I. Siro, D. Plackett, *Cellulose* **2010**, *17*, 459; c) M. Paakko, M. Ankerfors, H. Kosonen, A. Nykanen, S. Ahola, M. Osterberg, J. Ruokolainen, J. Laine, P. T. Larsson, O. Ikkala, T. Lindstrom, *Biomacromolecules* **2007**, *8*, 1934.
[26] A. F. Turbak, F. W. Snyder, K. R. Sandberg, *J. Appl. Polym. Sci.: Appl. Polym. Symp.* **1983**, *37*, 815.
[27] T. Zimmermann, E. Pöhler, T. Geiger, *Adv. Eng. Mater.* **2004**, *6*, 754.
[28] J. C. H. Wong, H. Kaymak, S. Brunner, M. M. Koebel, *Micropor. Mesopor. Mater.* **2014**, *183*, 23.
[29] a) H. Yu, S. L. Brock, *ACS Nano* **2008**, *2*, 1563; b) K. H. Kim, Y. Oh, M. F. Islam, *Adv. Funct. Mater.* **2013**, *23*, 377.
[30] J. Wang, Y. Wei, W. He, X. Zhang, X, *RSC Adv.* **2014**, *4*, 51146.
[31] Z. S. Deng, J. Wang, A. M. Wu, J. Shen, B. Zhou, *J. Non-Cryst. Solids* **1998**, *225*, 101.
[32] M. M. Koebel, A. Rigacci, P. Achard, in *Aerogels Handbook*, (Eds: M. A. Aergerter, N. Leventis, M. M. Koebel), Springer, New York **2011**, 607.
[33] Y. Kobayashi, T. Saito, A. Isogai, *Angew. Chem. Int. Ed.* **2014**, *53*, 10394.
[34] G. Hayase, K. Kanamori, K. Abe, H. Yano, A. Maeno, H. Kaji, K. Nakanishi, *ACS Appl. Mater Interfaces* **2014**, *6*, 9466.
[35] C. Rudaz, R. Courson, L. Bonnet, S. Calas-Etienne, H. Sallée, T. Budtova, *Biomacromolecules* **2014**, *15*, 2188.
[36] T. Stahl, S. Brunner, M. Zimmermann, K. Ghazi Wakili, *Energy Buildings* **2012**, *44*, 114.